Heat-Transfer Processes in Solar Energy Storage Systems for Orbital Applications

FRANK MARTINEK*
University of Vermont, Burlington, Vt.

A survey and study of the use of solar energy for power conversion systems for orbital missions confirmed the potential usefulness of heat storage systems utilizing the heat of fusion and the sensible heat of a material such as LiH. The properties of all surveyed candidate materials are temperature-dependent. The transient temperature distribution and the output heat flux q_0 are presented as functions of input heat flux q_i and the thickness w of the heat-storing material. The possibility of steady state without complete melting has been predicted and confirmed experimentally. The amplitude of the fluctuation in q_0 during the thermal cycle increases with q_i and w. The stabilization of the thermal cycle generally is achieved in two cycles (simulated orbital periods). Use of a finned system can reduce the q_0 fluctuations, including the temporary q_0 overshoots after the completion of melting. Changes of the fin geometry, spacing, and fin materials affect t_h and t_c. These additional degrees of freedom can be utilized for the synchronization of the thermal cycles with the orbiting periods. The theoretically predicted behavior of the system is in good agreement with experimental findings for annular storage volumes of LiH that are radiantly heated on the inside by an electric heater and cooled by radiation to Dowtherm-A-cooled or nitrogen-cooled coils.

Nomenclature†

g = gap between the fins, in.
H = enthalpy, Btu/lb
h = film heat-transfer coefficient, Btu/in.²-sec-°R
k = thermal conductivity, Btu/in.-sec°R
L = latent heat, Btu/lb
l = length, in.
M = mass, lb
N = number of nodes
n = normal unit vector, $|n| = 1$.
q = heat flux, Btu/in.²-sec
R = location of the fusion front, in.
r = radius position vector; $|r|$, in.
S = control surface, in.²
T = temperature, °R
t = time, sec
u = velocity of the mass, in./sec
V = volume, in.³
w = thickness of the heat storing material, in.; $w = (r_0 - \tau_0) - (r_i - \tau_i)$ for finless model
z = axial coordinate
Δ = finite difference increment
ϵ = emissivity
ρ = density, lb/in.³
τ_i, τ_0 = wall thicknesses of inner and outer cylinders

Superscripts

F,L,s = fusion front, liquid, and solid, respectively

Subscripts

c,h = cooling and heating, respectively
F,f = fusion front and fin, respectively
$i,0$ = inner and outer, respectively
n = number of the node; normal
N = last node
0 = reference time

Received June 25, 1969; revision received May 18, 1970. Extract from author's Ph.D. thesis at the University of Cincinnati.[1] The guidance, patience, and encouragement of W. Tabakoff of Aerospace Engineering Department is gratefully acknowledged.

* Associate Professor of Mechnical Engineering, University of Vermont. Associate Fellow AIAA.

† The meanings of the remaining subscript and superscripts are shown in Figs. 3 and 4.

Introduction

LARGE heat fluxes can be obtained for a spacecraft power system by collecting solar energy with parabolic mirrors. (Reference 1 includes a survey and study of this subject.) However, the day-night time periods during orbital missions limit the utilization potential of solar energy unless a portion of the energy collected is stored during the orbital day and released during the orbital night. The objectives of the present analysis are 1) to predict the behavior of such a heat storage using the heat of fusion, 2) to indicate the feasibility of synchronization of the thermal cycle with the orbital time, and 3) to establish the limiting operating conditions.

The first known discussion of heat conduction in media involving the change of phase is the Stefan's study[2] in 1891, and the problem is now commonly referred to as "Stefan's Problem." Some of the prior studies pertinent to the space power system usage are given in Refs. 3–7. Analytical solutions of the mathematical problem are limited to special cases because of the nonlinearity of differential equations. Numerical results can, however, be obtained with adequate accuracy

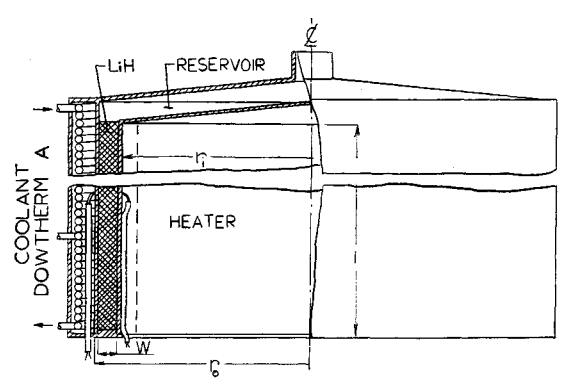

Fig. 1 Schematic of heat storage system without fins.

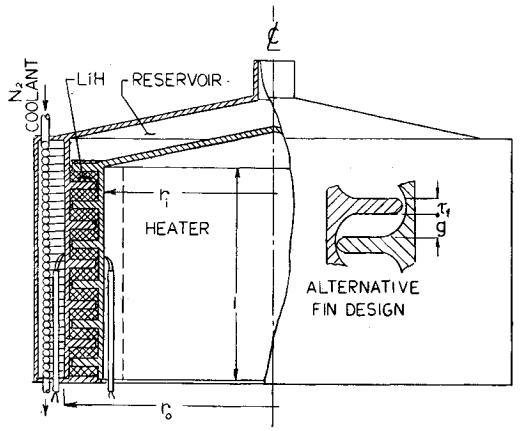

Fig. 2 Schematic of heat storage system with fins.

using high-speed digital computers.[8-10] Other studies pertinent to this problem are presented in Refs. 11–15.

Analysis of the Heat Storage System Involving Change of Phase

Fundamental Relationships

Let the control volume V containing the heat-storing material be bounded by a closed control surface S. Liquid and solid phases may exist simultaneously, within V; the material in each phase is, however, assumed to be homogenous and continuous. The physical, thermodynamic, and transport properties are assumed to be functions of the temperature T. The temperature at the solid-liquid interface is considered to be independent of time t and location r, and its value is assumed to correspond to the fusion temperature of the material T_F.

The thermal energy can be added or removed simultaneously across portions of the control surface. It is assumed there are no other heat sources or sinks except those caused by local changes of enthalpy during the transient states, and by the fusion process. Thermal fluxes q across the boundary surface are considered to be functions of time and location.

Table 1 summarizes the relationships derived from the conservation of mass, and Table 2 the relationships obtained from the conservation of energy.

Selected Mathematical Models

Two models have been considered. One assumes that the heat-storing material is contained in an annular volume

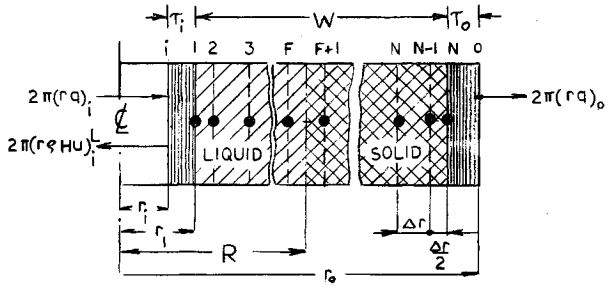

Fig. 3 Mathematical model of system without fins.

formed by two co-axial cylinders (Fig. 1), and the other includes heat-delivering and heat-rejecting fins (Fig. 2). Using cylindrical coordinates and converting the generalized relationships into finite differences, the mathematical models in Figs. 3 and 4 result.

For the model without fins it is assumed that: w is independent of the temperature; a reservoir is provided for the accommodation of excess material resulting from the density changes; thermal equilibrium exists in the reservoir; transport of the excess material does not affect the heat flows; and transport properties of the walls are known functions of the temperature.

Two primary assumptions for the model with fins are: heat is delivered into the system only by the fins connected to the inner wall, and it is released from the system only by the fins connected to the outer wall. These two assumptions can approach realistic conditions of operation if the fin geometry is modified as shown in Fig. 2. In addition, it is assumed that the fins are thin and made of material of high thermal diffusivity; that the gaps between the fins and opposite walls are small, but the heat flow across these gaps is negligible; and that there is no mass transfer between the adjoining volumes (i.e., each volume formed by the heat-delivering and heat-rejecting fin is a discrete volume with allowance for the thermal expansion of the heat-storing material).

Predicted Behavior of System

Storage System without Fins

The inner diameter of the container was held constant (9 in.). Radiation to a zero-temperature environment is the heat-rejecting mechanism. The input heat flux q_i and the width w of the annular space were considered as independent parameters. The emissivity ϵ of the heat-rejecting wall was assumed to be 0.9, and the view factor, unity.

Table 1 Equations of continuity-conservation of mass. $\Delta z = 1$

Phase	Mass flow across the surface	
Solid	$\iint_{{}^sS} {}^s(\rho\mathbf{u})\cdot\mathbf{n}dS = \sum^{s} \iint_{{}^sS_2} (\rho\mathbf{u})\cdot\mathbf{n}dS - \sum \iint_{{}^sS_1} {}^s(\rho\mathbf{u})\cdot\mathbf{n}dS + \iiint_{{}^sV} \frac{\partial {}^s\rho}{\partial t}\, dV$	(1)
	$\iint_{{}^sS_F} {}^s(\rho\mathbf{u})^F\cdot\mathbf{n}dS = \sum^{F} \iint_{{}^sS_2} {}^s(\rho\mathbf{u})\cdot\mathbf{n}dS - \sum^{F} \iint_{{}^sS_1} {}^s(\rho\mathbf{u})\cdot\mathbf{n}dS + \iiint_{{}^sV_F} \frac{\partial {}^s\rho}{\partial t}\, dV$	(2)
Liquid	$\iint_{{}^LS} {}^L(\rho\mathbf{u})\cdot\mathbf{n}dS = \sum \iint_{{}^LS_1} {}^L(\rho\mathbf{u}_L)\cdot\mathbf{n}dS - \sum \iint_{{}^LS_2} {}^L(\rho\mathbf{u})\cdot\mathbf{n}dS - \iiint_{{}^LV} \frac{\partial {}^L\rho}{\partial t}\, dV$	(3)
	$\iint_{{}^LS_F} {}^L(\rho\mathbf{u})^F\cdot\mathbf{n}dS = \sum^{F} \iint_{{}^LS_1} {}^L(\rho\mathbf{u})\cdot\mathbf{n}dS - \sum^{F} \iint_{{}^LS_2} {}^L(\rho\mathbf{u})\cdot\mathbf{n}dS - \iiint_{{}^LV_F} \frac{\partial {}^L\rho}{\partial t}\, dV$	(4)
Mass velocity of the liquid near the fusion front		
Liquid	${}^L\mathbf{u}_F = \left(\frac{{}^s\rho}{{}^L\rho}\right)_F {}^s\mathbf{u}_F - \left(\frac{{}^s\rho - {}^L\rho}{{}^L\rho}\right)\mathbf{u}_F$	(5)

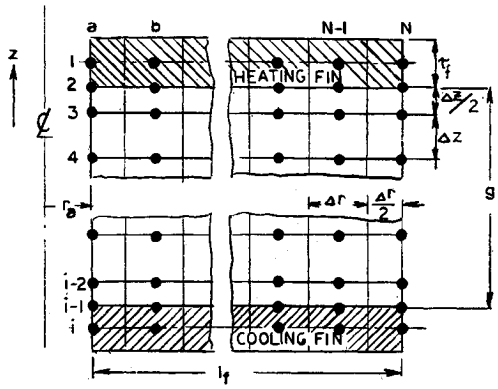

Fig. 4 Mathematical model of system with fins.

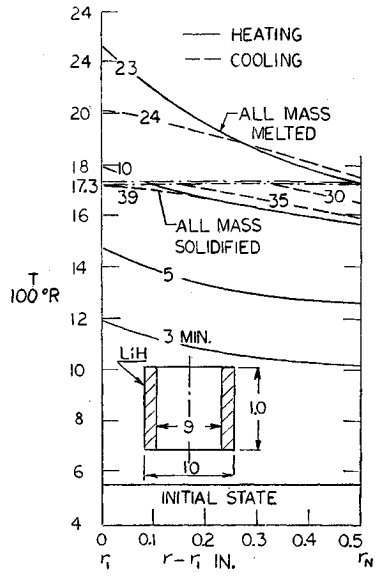

Fig. 5 Computed LiH temperature profiles in system without fins; r_1 = 4.5 in.; q_i = 0.05 Btu/in.²-sec; ϵ = 0.9.

The temperature history within the storage material is shown in a typical case (Fig. 5) for q_i = 0.05 Btu/in.²-sec and $w = \frac{1}{2}$ in. As the temperature increases, the temperature gradients also rise due to the reduced thermal diffusivity of LiH. The initial temperature rise is rapid. The melting process reduces dT_i/dt. When all material is melted ($T_0 = T_F$ = 1730°R), q_i is reduced to zero. During the initial cooling period T_i falls rapidly, while T_0 continues to rise for some time. When T_0 falls again to 1730°R, solidification begins and progresses toward the inner boundary. The temperature of the remaining molten material remains nearly constant (1730°R), while the temperature within the solidified layer gradually decreases.

Figures 6a and 6b show T_i for three values of q_i at each of two values of w. These results represent the initial cycle of operation. The temperature peaks occur at the end of the orbital day. The variation of T_0 and q_0 ($\propto T_0^4$) for the same case as Fig. 6a are shown in Fig. 7. The T_0 overshoot after the material has melted and the power source has been withdrawn results from the temperature gradients within the system at the end of the simulated orbital day. The larger q_i is, the larger the overshoot is. The value of the peak T_0 is nearly independent of w, but the duration of the overshoot increases with increased w.

Thermal Cycling of LiH Storage System without Fins

The time period t_p of the initial cycle is defined as the sum of the time t_h needed for the heating of the system from its initial state until all material just melts and the time t_c required for the system to cool until all material just solidifies. If the final state of the first cycle is taken as the initial state of the second cycle, and if the process is repeated a sufficient number of times, the thermal cycling becomes stabilized; i.e., the effect of the initial state of the first cycle is no longer felt.

Figure 8 shows the variation of q_0 assuming that q_i = 0.1 Btu/in.²-sec, w = 0.5 in., and that the system was initially at 560°R. The first cycle period t_{p1} is longer than the period of subsequent cycles. For this high q_i case, the second cycle can already be considered stabilized ($t_{p2} = t_{p3} = t_{p4}$ = 25 min). The q_0 overshoot in this case represents 40% of the total power fluctuation of the stabilized cycle. The stabilization of the distribution within the system however, requires several cycles. This is the consequence of the mathematical model of constant volume in which it is assumed that the expanding material at the time-dependent temperature T_i is stored, temporarily, in an adiabatic reservoir, where it reaches thermal equilibrium. Consequently, the enthalpy of the material in the reservoir will always be lower than the instantaneous enthalpy of the mass entering it during the heating period. During the cooling period the enthalpy of the mass re-entering the main storage (control) volume V corresponds to the final temperature in the reservoir. However, the stabilization of the energy distribution within the system is already achieved during the third cycle.

Table 2 Equations of heat conduction assumption: $\Delta z = 1$

Phase	Energy flux across the surface S	
Solid	$\iint_{{}^sS} (\mathbf{q} + \rho H\mathbf{u})^s \cdot \mathbf{n} dS = \sum \iint_{{}^sS_2} (\mathbf{q} + \rho H\mathbf{u})^s \cdot \mathbf{n} dS - \sum \iint_{{}^sS_1} (\mathbf{q} + \rho H\mathbf{u})^s \cdot \mathbf{n} dS + \iiint_{{}^sV} \frac{\partial}{\partial t} (\rho H)^s dV$	(6)
	$\iint_{{}^sS_F} (\mathbf{q} + \rho H\mathbf{u})^s \cdot \mathbf{n} dS = \sum^F \iint_{{}^sS_2} (\mathbf{q} + \rho H\mathbf{u})^s \cdot \mathbf{n} dS - \sum^F \iint_{{}^sS_1} (\mathbf{q} + \rho H\mathbf{u})^s \cdot \mathbf{n} dS + \iiint_{{}^sV_F} \frac{\partial}{\partial t} (\rho H)^s dV$	(7)
Liquid	$\iint_{L_S} (\mathbf{q} + \rho H\mathbf{u})^L \cdot \mathbf{n} dS = \sum \iint_{L_{S_1}} (\mathbf{q} + \rho H\mathbf{u})^L \cdot \mathbf{n} dS - \sum \iint_{L_{S_2}} (\mathbf{q} + \rho H\mathbf{u})^L \cdot \mathbf{n} dS - \iiint_{L_{V_F}} \frac{\partial}{\partial t} (\rho H)^L dV$	(8)
	$\iint_{L_{S_F}} (\mathbf{q} + \rho H\mathbf{u})_F{}^L \cdot \mathbf{n} dS = \sum^F \iint_{L_{S_1}} (\mathbf{q} + \rho H\mathbf{u})^L \cdot \mathbf{n} dS - \sum^F \iint_{L_{S_2}} (\mathbf{q} + \rho H\mathbf{u})^L \cdot \mathbf{n} dS - \iiint_{L_{V_F}} \frac{\partial}{\partial t} (\rho H)^L dV$	(9)
	Velocity of the fusion front and of the liquid in the vicinity of the fusion front	
Fusion	$\mathbf{u}_F = {}^s\mathbf{u}_F - \left(\frac{{}^sq - {}^Lq}{{}^s\rho^L}\right)_F = {}^s\mathbf{u}_F - \frac{{}^L(k\nabla T)_F - {}^s(k\nabla T)_F}{{}^s\rho_F{}^L}$	(10)
Liquid	${}^L\mathbf{u}_F = {}^s\mathbf{u}_F + \left(\frac{{}^s\rho - {}^L\rho}{{}^s\rho}\right)_F \left(\frac{{}^Lq - {}^sq}{{}^s\rho^L}\right) = {}^s\mathbf{u}_F - \frac{{}^L(k\nabla T)_F - {}^s(k\Delta T)_F \left(\frac{{}^s\rho - {}^L\rho}{{}^s\rho}\right)_F}{{}^s\rho_F{}^L}$	(11)

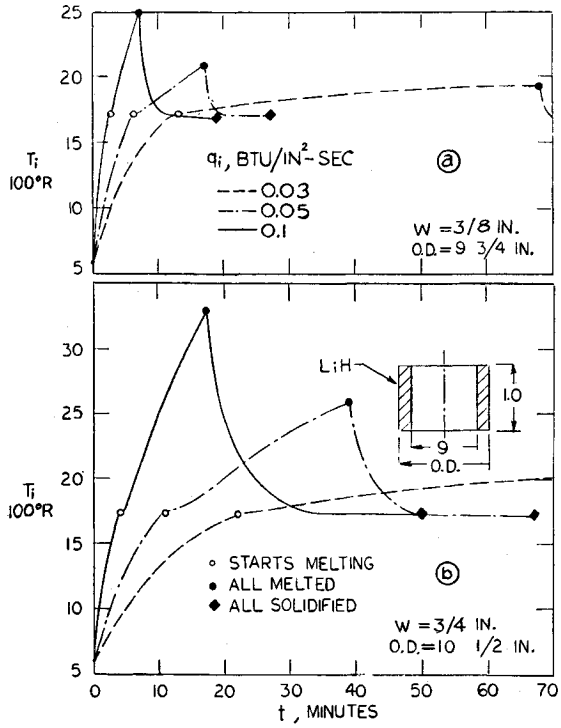

Fig. 6 Computed temperature at inner boundary T_i during the initial cycle for three values of q_i at each of two LiH thicknesses w; $\epsilon = 0.9$.

Storage System with Fins

For the results presented, the outer and the inner diameters of the container, the gap between the fins, and the input power are variable parameters, while the fin length (1 in.) and thickness (0.2 in.) are kept constant. The properties of the fin material correspond to 316 stainless steel. In all cases the computed temperature profiles in the fins and within the heat-storage material are similar. The locations of the isothermal fusion front during melting and solidification periods are shown in Fig. 9. The effect of high thermal diffusivity of the fins as compared with that of LiH is clearly discernible at the fin-heat storage boundaries.

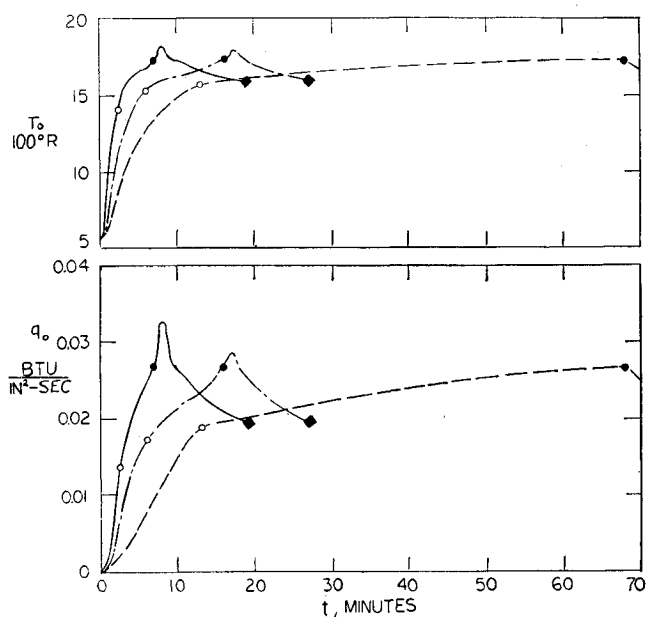

Fig. 7 Computed temperature T_0 and heat flux q_0 at outer boundary for operating conditions stated in Fig. 6.

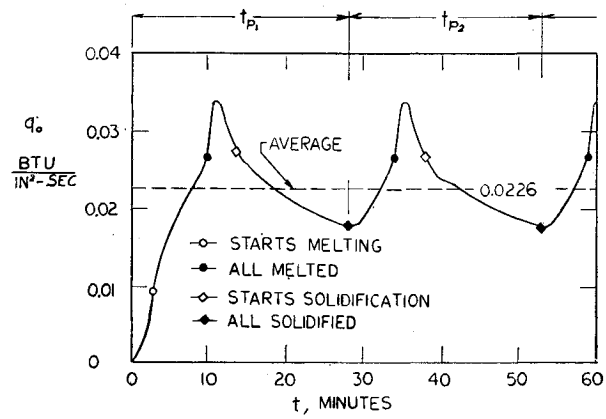

Fig. 8 Predicted q_0 from the system without fins; $q_i = 0.1$ Btu/in.²-sec; $w = 0.5$ in.; initial temperature = 560°R.

The predicted output heat fluxes are shown in Fig. 10 for $q_i = 0.05$ Btu/in.²-sec, $g = \frac{1}{4}$ in. and $\tau_f = 0.2$ in. The thermal cycling is stabilized for all practical purposes during the second orbit ($t_{p_2} = t_{p_3} = 71.3$ min). The cooling period is nearly constant from the initial cycle ($t_{c_1} = t_{c_2} = 11.8$ min).

The q_0 rise from the system is not uniform. Initially the fusion front is relatively far from the heat sink, and the q_0 rise is less than in the final stage of melting. After q_i is removed, q_0 decreases rapidly, and q_0 overshoot is negligible. In the presented case the average q_0 is 3.36×10^{-2} Btu/in.²-sec; the extrema oscillate around this average by +10.8% and −10.2%. Subsequent investigation indicated that t_p depends much more strongly on q_i than on w.

Experimental Program

Model without Fins

For this model (Fig. 1), the ratio of the length to the width (w) of the annular LiH volume was large (26) to minimize the end effects; the upper ends of the cylinders were free to expand in the axial direction. The heat-storage volume was closed by cone-shaped covers providing a reservoir for the expanding LiH. A series of 5 Dowtherm-A-cooled, copper coils formed the heat sink.

The inner cylinder, closed on the upper end, formed the cavity in which was placed the electrical resistance heater. Chromel-Alumel thermocouples were distributed over the inner and the outer walls of the LiH container (Figs. 1 and 2). Dowtherm A was selected for cooling because it is one of the candidate fluids for the dynamic power conversion system for space. The system was insulated from the environment by radiation shields and 2-in.-thick asbestos wool. The thermal losses from the system were determined experimentally. These losses were taken into account when the comparison was made between the predicted and experimentally found values.

The analysis predicted that complete melting of LiH cannot be attained with power inputs below 9 kw. An experiment 8 kw confirmed this prediction, because T_0 reached

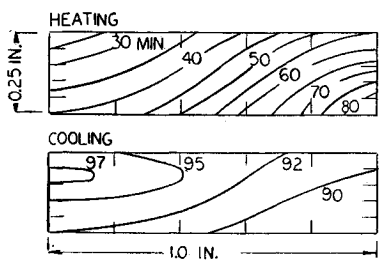

Fig. 9 Predicted location of fusion front in system with fins; $q_i = 0.05$ Btu/in.²-sec; $\tau_f = 0.20$ in.; $g = 0.25$ in.; $r_1 = 4.5$ in.; $r_N = 5.5$ in.; Fin material, stainless steel 316.

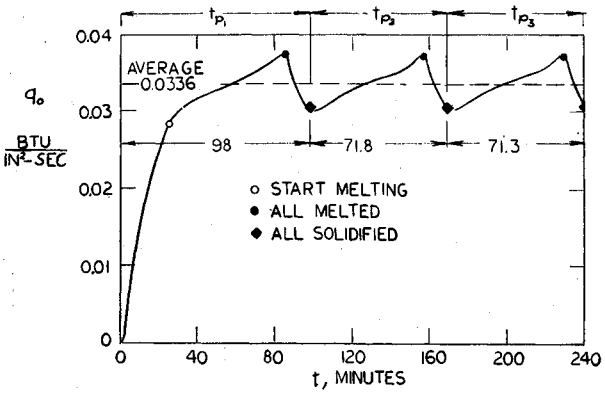

Fig. 10 Predicted q_0 from the system with fins for operating conditions stated in Fig. 9.

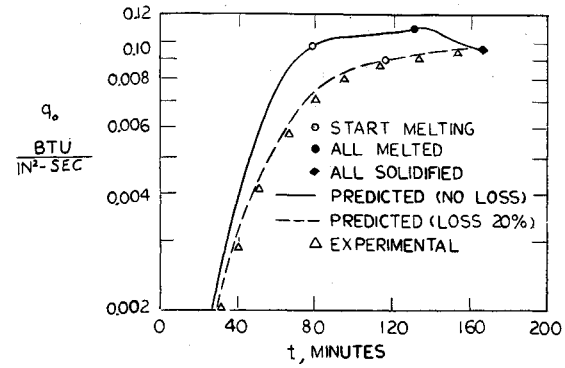

Fig. 12 Predicted and experimental q_0 from the system with fins; $q_i = 1.7 \times 10^{-2}$ Btu/in.²-sec.

1655°R after 100 min. and remained steady thereafter, even though T_i passed T_F (1730°R) at 65 min. and remained steady at 1830°R after 98 min. Thus, only a partial melting was accomplished indicating one of the constraints of performance.

Additional experiments were performed at q_i = 9, 10, 11, and 12 kw. Typical results obtained at q_i = 12 kw are presented in Fig. 11. Close agreement between the predicted and measured T_i can be seen during the first hour. After that time the experimental T_i's are lower than predicted values. This difference can be explained by the convective currents of molten mass from the region near the storage base (end losses) to the upper region where the actual data were taken. The mathematical model predicted that the material would be completely molten after 133 min. The discrepancy can again be attributed to the cooling effect of the mass currents from the lower regions of the system. An additional 27 min were needed to melt the material near the base (experimental overrun). The slightly lower experimental rate of cooling after power removal can be attributed to the convective mass flow from the reservoir to the base of the system.

The predicted and measured T_0's differ significantly during the initial heating, but are in good agreement during the time

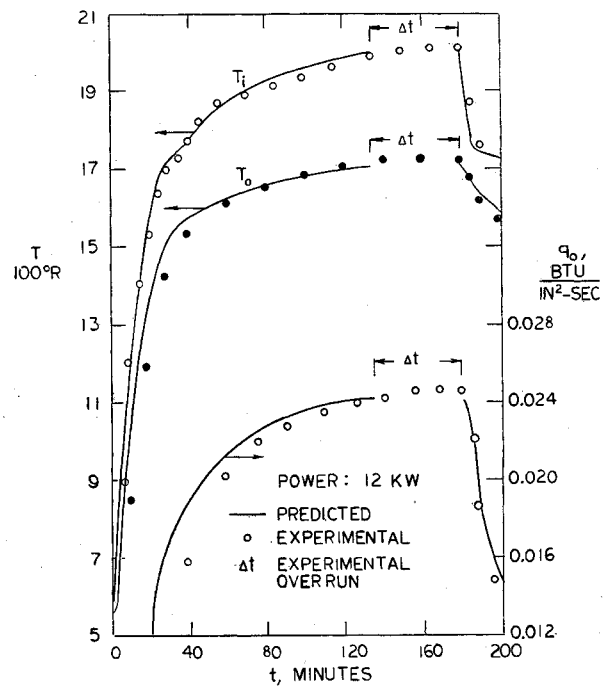

Fig. 11 Predicted curves and experimental data points for T_0, T_i, and q_0 in system without fins during the first cycle; power input 12 kw, r_i = 4.5 in.; w = 0.5 in.

of melting. The q_0's were calculated from the flow rate of the coolant (Dowtherm A) and its enthalpy rise. Since $q_0 \propto T_0^4$, the lag of the experimental q_0 is more pronounced than the lag of the experimental T_0 (Fig. 11).

Model with Fins (Fig. 2)

The volume of the LiH storage was formed by $\frac{3}{4}$-in. annular space formed by coaxial cylinders of 10.5 in. and 9 in. diam, respectively. The 0.2-in.-thick fins were evenly spaced (g = 0.35 in.). Stainless steel 316 was used for the container and the fins. The design allowed free axial expansion of both cylinders. The heat sink was formed by a tight coil tubing through which passed the cooling fluid (nitrogen). The inner wall of the storage, closed on the upper end, formed the receptacle for the heater.

The power flux into the system was maintained at 1.7×10^{-2} Btu/in.²-sec. The experimental q_0's are compared with the predicted values in Fig. 12. The experimentally-found thermal losses from the system at 1730°R were approximately 20% of the power input.

Conclusions and Summary

The conclusions, based on results of this study, can be summarized as follows.

1) The control of the distribution of the absorbed solar flux to the heat-storage walls is important: High power fluxes can result in prohibitive temperatures of the heat-storing material as well as of the materials of the structure (Figs. 6a, b).

2) When the properties of the heat-storage material are dependent on the temperature, the system becomes dynamic; i.e., the convective fluxes of the mass and of the energy associated with them cannot be neglected. A suitable expansion volume must be provided for the accommodation of the excess material volume.

3) In a heat-storage system of simple cylindrical configuration, and in the range of moderate power inputs, the solidification time of the material of a fixed annular thickness w varies little with the input, but greater w increases both the heating and cooling times. The fluctuations in output heat flux q_0 remain large even after the thermal cycle has stabilized (after two or more cycles). These fluctuations increase with increase in w and q_i. A q_0 overshoot occurs after the material has just melted because of the large temperature gradients that remain within the system after q_i is discontinued. The excursions in q_0 possibly could be reduced by discontinuing q_i before the fusion front reaches the outer boundary.

4) The low limit for q_i is that for which all of the material is just melted when the system reaches a steady state; with a lower q_i, the heat-storing capacitance of the system is not fully utilized.

5) The heating period of the initial cycle is longer than that of the following cycles. The cooling period of the initial

and of the subsequent cycles varies to a lesser extent. The heat stored within the system and the heat released from it per cycle converge rapidly toward the stabilized cycle values.

6) The addition of interdigitated heat-conducting fins to the heat-storage system reduces the q_0 excursions at the end of the melting. The energy stored in the material of the fins cannot be neglected, but the additional degrees of freedom provided by the choices of fin material, make it possible to synchronize the thermal cycling of the system with orbital cycles.

References

[1] Martinek, F., "Investigation of Heat Transfer Process in Solar Energy Storage Systems for Space Applications," Ph.D. thesis, 1966, Univ. of Cincinnati.

[2] Stefan, J., "Ueber die Theorie der Eisbildung in Polarmeere," *Annalen der Physik and Chemie*, Vol. 42, 1891, p. 269

[3] Altman, M., "Prospects for Thermal Energy Storage," *AGARD'ograph 81*, Gordon & Breech, New York, 1967, pp. 135–149.

[4] Altman, M., "The Determination of Thermal Energy Diffusivities of Thermal Energy Storage Materials," *Transactions of the ASME, Ser. A: Journal of Engineering for Power*, Vol. 89, 3, July 1967, pp. 407–414.

[5] Cygnarowicz, T. A. and Gibson, R. N., "Design and Performance of a Thermal Storage Resistoret," *Journal of Spacecraft and Rockets*, Vol. 5, No. 6, June 1968, p. 686.

[6] Sutton, G. W., "The Hydrodynamics and Heat Conduction of a Melting Surface," *Journal of the Aerospace Sciences*, Vol. 25, No. 1, Jan. 1958, pp. 29–32.

[7] Tripp. C. N., "Volatile Liquid Pressurization," *Journal of Spacecraft and Rockets*, Vol. 5, No. 12, Dec. 1968, p. 1477.

[8] Douglas, J., and Gallie, T. M., "On the Numerical Integration of a Parabolic Differential Equation Subject to a Moving Boundary Condition," *Duke Math. Journal*, Vol. 22, 1955, Duke Univ., Durham, N. C., p. 577.

[9] Murray, W. D., "Numerical and Machine Solutions of Problems in Transient Heat Conduction," Ph.D. thesis, 1958, New York Univ., College of Engineering.

[10] Price, P. H. and Slack, M. R., "Stability and Accuracy of Numerical Solutions of Heat Flow," *British Journal, Applied Physics*, Vol. 3, 1952, p. 379.

[11] Citron, S. J., "Heat Conduction in a Melting Slab," Ph.D. thesis, 1959, Columbia Univ.

[12] Cochran, D. L., "Rate of Solidification, Application and Extension of Theory." T-R 24, Contract N6NONr-251, 1955, Stanford Univ., Stanford, Calif.

[13] Evans, G. W., Isaacson, E., and MacDonald, J. K. L., "Stefan-like Problems," *Quarterly of Applied Mathematics*, Vol. 8, 1950, pp. 312–319.

[14] Hrycak, P., "Problem of Solidification with Newton's Cooling at the Surface," *AIChE Journal*, Vol. 9, No. 5, 1963, pp. 585–589.

[15] Ruoff, A. L., "An Alternare Solution of Stefan's Problem," *Quarterly of Applied Mathematics*, Vol. 16, July, 1958, pp. 197–201.

SEPTEMBER 1970 J. SPACECRAFT VOL. 7, NO. 9

Aerodynamic First-Order Method for Flexible Bodies

GEORGE F. MCCANLESS JR.*
Chrysler Corporation, Huntsville, Ala.

This paper develops an advanced method of computing aerodynamic forces that act on flexible launch vehicles and missiles in supersonic flight. The procedure is an extension of the rigid-body, first-order method. The equation of the perturbation velocity potential is first expressed in rigid Cartesian coordinates. It is then transformed into flexible-body coordinates to simplify the boundary conditions. The transformed aerodynamic boundary value problem for flexible bodies is solved to yield the stream velocities at body surfaces. The velocities then determine the surface pressures and hence the body forces. Sample calculations for a flexed cone and for a flexed Saturn V vehicle demonstrate that significant aerodynamic forces are induced by forebody flexing.

Nomenclature

a_i = constants of the supersonic source strength derivatives, fps
b_i = constants of the supersonic doublet strength derivatives, fps
C_N = normal force coefficient
C_p = pressure coefficient
D = base diameter, ft
f = supersonic source strength, ft²/sec
m = supersonic doublet strength, ft²/sec
M = Mach number
M_{cg} = pitching moment about the center of gravity, ft lb
N = normal force, lb
N' = local normal force, lb/ft
p = arbitrary point in space
q = dynamic pressure, lb/ft²
r = radial coordinate in flexible-body coordinate system, ft
R = body radius, ft
s = dummy integration variable
U,u = velocities in the X and x directions, fps
V,v = velocities in the Y and r directions, fps
W,w = velocities in the Z and θ directions, fps
x = flexible-body axial coordinate, ft
X,Y,Z = Cartesian coordinates, ft
$\bar{Z}$ = displacement of flexible-body axis in the cartesian coordinate system, ft
α = local angle of attack, rad
α_r = rigid-coordinate angle of attack, rad
β = Mach number parameter
γ = specific heat ratio
θ = flexible-body circumferential coordinate, rad
$\Lambda_{n,i}$ = parameter defined by Eq. (25)
ν = number of body stations
$\Xi_{n,i}$ = parameter defined by Eq. (26)
ϕ = perturbation velocity potential, ft²/sec

Received June 16, 1969; revision received March 31, 1970. This study was supported by the Aero-Astrodynamics Laboratory of NASA Marshall Spaceflight Center under contract NAS8-21290. J. G. Papadopoulos was the program Contracting Officer's Representative.

* Engineering Specialist. Member AIAA.